2015

Development and validation of the global surface type data product from S-NPP VIIRS

Rui Zhang
University of Maryland, zhangrui@umd.edu

Chengquan Huang
University of Maryland, cqhuang@umd.edu

Xiwu Zhan
Center for Satellite Applications and Research, NESDIS/NOAA, College Park

Qin Dai
University of Maryland

Kuan Song
University of Maryland

REMOTE SENSING LETTERS, 2016
VOL. 7, NO. 1, 51–60
http://dx.doi.org/10.1080/2150704X.2015.1101649

Taylor & Francis
Taylor & Francis Group

Development and validation of the global surface type data product from S-NPP VIIRS

Rui Zhang[a], Chengquan Huang [a], Xiwu Zhan[b], Qin Dai[a,c] and Kuan Song[a]

[a]Department of Geographical Sciences, University of Maryland, College Park, USA; [b]Center for Satellite Applications and Research, NESDIS/NOAA, College Park, USA; [c]Institute of Remote Sensing and Digital Earth, Chinese Academy of Sciences, Beijing, China

ABSTRACT

Accurate representation of actual terrestrial surface types at regional to global scales is an important element for many applications. Based on National Aeronautics and Space Administration Moderate Resolution Imaging Spectroradiometer land cover algorithms, a global surface-type product from observations of the Visible Infrared Imaging Radiometer Suite (VIIRS) on board the Suomi National Polar-orbiting Partnership, provides consistent global land cover classification map for various studies, such as land surface modelling for numerical weather predictions, land management, biodiversity and hydrological modelling, and carbon and ecosystem studies. This letter introduces the development and validation of the VIIRS global surface-type product using the land cover classification scheme of the International Geosphere-Biosphere Programme. Surface reflectance data from VIIRS were composited into monthly data and then into annual metrics. The C5.0 decision tree classifier was used to determine the surface type for each pixel in a 1 km grid. To quantitatively evaluate accuracies of the new surface type product, a visual interpretation-based validation was performed in which high-resolution satellite images and other ancillary data were used as the reference. The validation result based on the large validation data set indicated that (78.64 ± 0.57)% overall classification accuracy was achieved.

ARTICLE HISTORY
Received 15 June 2015
Accepted 25 September 2015

1. Introduction

Global mapping of land cover is critical for a wide range of applications, such as land surface parameterization (Feddema 2005), modelling of biogeochemical cycles (Cramer et al. 1999) and carbon cycle studies (Friedlingstein et al. 2006). Since the 1990s, a variety of global surface-type products with different spatial resolutions and legend definitions have been introduced into the scientific community. The best-known land cover products include International Geosphere-Biosphere Program (IGBP) DISCover, created using 1992–1993 1 km resolution Advanced Very High Resolution Radiometer (AVHRR) data (Loveland et al. 1999), the University of Maryland (UMD) land cover product, which was also based on the 1 km AVHRR data (Hansen et al. 2000), Global Land Cover 2000 (Bartholomé and Belward 2005) by the Joint Research Centre of the European

CONTACT Rui Zhang zhangrui@umd.edu

Commission, which was generated using the 2000 VEGETATION sensor on board Satellite Pour l'Observation de la Terre 4 satellite, and the Moderate Resolution Imaging Spectroradiometer (MODIS) land cover product using MODIS-based surface reflectance data (Friedl et al. 2010).

With the launch of the Suomi National Polar-orbiting Partnership (S-NPP) satellite on 28 October 2011, and the data from the Visible Infrared Imaging Radiometer Suite (VIIRS) on board S-NPP having become available since early 2012, the National Oceanic and Atmospheric Administration (NOAA) Joint Polar Satellite System (JPSS) land surface-type team began generating a new global surface-type classification map using the new VIIRS data. Here, the term 'surface type' is a renaming of the 'land cover' in the JPSS S-NPP program. The VIIRS global surface-type map followed the definition of the 17 IGBP classes (Herold et al. 2008), with approximately 1 km spatial resolution. The C5.0 decision tree algorithm, which was inherited from MODIS land cover development, was employed as the main classification algorithm to produce the global map. Daily surface reflectance data were composited into monthly data, and then a series of annual metrics was generated for input to the classifier. This entire process generally followed the approach used by the MODIS land cover products (Friedl et al. 2010). The VIIRS global gridded surface-type (GST) classification map, also known as surface-type intermediate product in the JPSS level 1 requirement document (NOAA 2014b), is the base layer in the surface type environmental data record product (EDR), in which dynamic snow/ice and active fire flags are incorporated on top of the classification map. The surface-type EDR will be produced for every acquired set of VIIRS granule data, but the classification map (GST) will be updated once a year, which is adequate and practical based on experiences learned from developments of the MODIS land cover products.

In this letter, the development and validation of VIIRS surface-type map are presented. The validation results suggested that the new VIIRS surface-type classification map achieved (78.64 ± 0.57)% overall correct rate, which exceeded the accuracy requirement of 70% for this product defined in the JPSS level 1 requirement document.

2. Development of the VIIRS global surface-type classification map

2.1. *VIIRS data processing*

The VIIRS sensor represents a continuation of National Aeronautics and Space Administration (NASA)'s Earth Observing System MODIS sensors and NOAA's Polar Orbiting Environmental Satellites AVHRR sensors. The VIIRS has five high-resolution imagery bands (I-bands) with a nadir resolution of 375 m and 16 moderate resolution bands (M-bands) with 750 m resolution. In addition, a 750 m day/night band (DNB), which provides low-light night-time sensing capability, is designed to replace Operational Linescan System instruments on board Defense Meteorological Satellite Program satellites. The VIIRS band information is listed in Table 1 (Lee et al. 2006), and the bands used in surface-type generation are shown in bold.

2012 VIIRS reflectance data from bands M1 to M11 (excluding M6 and M9) and the brightness temperature of band M14 were downloaded from NASA's Level 1 and Atmosphere Archive and Distribution System, reprojected into sinusoidal projection and mosaicked into global daily data. Data from 32 consecutive days were then

Table 1. VIIRS band information.

Band	Wavelength (μm)	Band	Wavelength (μm)
M1	0.412	M9	1.38
M2	0.445	**M10**	1.61
M3	0.488	I3	1.61
M4	0.555	**M11**	2.25
I1	0.64	M12	3.7
M5	0.672	I4	3.74
M6	0.746	M13	4.05
I2	0.865	**M14**	8.55
M7	0.865	M15	10.76
DNB	0.7	I5	11.45
M8	1.24	M16	12.01

Note: The bolded bands were used for surface-type classification.

composited into 32-day data that represented monthly reflectance conditions. Maximum normalized difference vegetation index (NDVI) value composite procedure was used to generate the composite data (Holben 1986). The compositing processes were used to remove residual cloud, cloud shadow and anomaly data and other noises. Annual metrics were then created from 32-day composite data, which followed the method that Hansen et al. (2000) proposed for producing the UMD land cover data. The generated 69 annual metrics are listed in Table 2.

Annual metrics used in the VIIRS surface-type algorithm include the maximum, minimum, mean and amplitude values calculated using the monthly composites of the eight greenest months of the past 12 months. Use of the eight greenest months instead of all 12 months of a calendar year to calculate these metrics effectively reduces the complications caused by seasonal snow cover and yet retains the seasonal variability associated with vegetation phenology. The eight greenest months are not necessarily consecutive, but represent the 8 months with the clearest view of green vegetation. Another two sets of metrics include individual monthly composite values of the greenest month indicated by the highest monthly NDVI value and the warmest month indicated by highest monthly M14 brightness temperature. Another set of metrics is calculated using the mean value of four warmest months as measured by monthly M14 brightness temperature to capture some of the information not included in the eight greenest months. The four warmest months were found to be associated with the dry season or

Table 2. Details of annual metrics used in classification.

Metrics number(s)	Description
1	Maximum NDVI value
2	Minimum NDVI value of eight greenest months
3	Mean NDVI value of eight greenest months
4	Amplitude of NDVI over eight greenest months
5	Mean NDVI value of four warmest months
6	NDVI value of warmest month
7,14,21,28,35,42,49,56,63	Maximum band *x* value of eight greenest months
8,15,22,29,36,43,50,57,64	Minimum band *x* value of eight greenest months
9,16,23,30,37,44,51,58,65	Mean band *x* value of eight greenest months
10,17,24,31,38,45,52,59,66	Amplitude of band *x* value over eight greenest months
11,18,25,32,39,46,53,60,67	Band *x* value from month of maximum NDVI
12,19,26,33,40,47,54,61,68	Mean band *x* value of four warmest months
13,20,27,34,41,48,55,62,69	Band *x* value of warmest month

Note: *x* is the band used in annual metrics, which includes M1, M2, M3, M4, M5, M7, M8, M10 and M11.

the senescent phase of tropical vegetation. Using this set of metrics allows data not included in the eight greenest months to be used for some areas without introducing snow values at high latitudes and elevations.

2.2. *Classification*

In this study, training sites data provided by the MODIS land cover team were used to extract training samples from the VIIRS annual metrics for the training process. After removing urban and water samples, which were not involved in the training, small portions of additional croplands and cropland/natural vegetation mosaic samples were included into the training data. All newly added training areas were visually inspected against Google Earth high-resolution images. Details of the training samples are listed in Table 3. Urban and built-up (class 13) pixels were not labelled in the classification process, but assigned using a separate urban extent data (Schneider, Friedl, and Potere 2009). Therefore, the number of training samples for this class is zero in Table 3. Similarly, water body pixels were mapped from an existing land/water mask, which was introduced in Carroll et al. (2009).

The S-NPP VIIRS surface-type map was produced using the C5.0 decision tree classifier (Quinlan 2004). Boosting technique (Freund and Schapire 1997) in the C5.0 package, which is designed to improve the predictive accuracy by combining multiple trees, was used in the map classification. Because the C5.0 decision tree classification algorithm is

Table 3. Number of training and validation samples, validation sample distribution and area proportions in classified map for each class.

IGBP class number	IGBP class name	Number of observations in training sample	Number of observations in validation sample	Validation sample allocations (%)	Area in classified map (%)
1	Evergreen needleleaf forests	481	164	4	2.24
2	Evergreen broadleaf forests	1051	491	10	9.68
3	Deciduous needleleaf forests	177	104	2	1.24
4	Deciduous broadleaf forest	631	210	3	0.81
5	Mixed forests	747	270	6	6.28
6	Closed shrublands	369	111	2	0.06
7	Open shrublands	1106	497	11	16.64
8	Woody savannahs	920	559	11	8.65
9	Savannahs	829	357	5	8.39
10	Grasslands	1720	562	12	8.78
11	Permanent wetlands	1241	42	1	1.15
12	Croplands	4038	752	16	7.59
13	Urban and built-up lands	0	98	2	0.43
14	Cropland/natural vegetation mosaics	1283	411	9	4.29
15	Snow and ice	180	45	1	10.88
16	Barren	851	285	5	12.89
Total		15,624	4958	100	100

Note: Water bodies class (17) is not included.

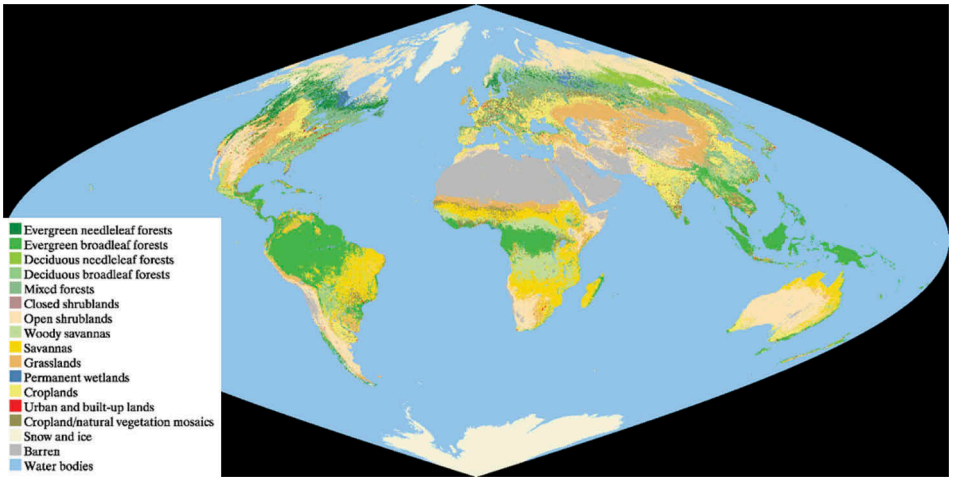

Figure 1. Delivered VIIRS global surface-type classification map in 17 IGBP classes.

generally well known and has been utilized by many previous land cover products, the mathematical equations of the C5.0 are not included in this letter. The technical details may be found from Quinlan (1993, 2004). The processing steps of creating the S-NPP VIIRS surface-type map were similar to those from the MODIS collection 5 land cover product. A boosted decision tree (or classification model) was applied to the annual metrics (input variables), and the IGBP labels were predicted in the classification process. MODIS collection 5 land cover used 3-year classification results to stabilize the final class labels (Friedl et al. 2010), but the S-NPP VIIRS did not include this step due to limited data availability. Detailed descriptions of the entire classification process may be found in the JPSS Algorithm Theoretical Basis Document for the VIIRS surface-type product (NOAA 2014a).

After the initial classification map was obtained, multiple post-classification processes were applied to improve the quality of the surface-type map, which included filling in unclassified ocean pixels and missing high-latitude regions. In addition, a crop probability product from a global cropland extent project was used to help reassign portions of cropland labels if high crop probability was identified (Pittman et al. 2010). After post-classification processes, the final VIIRS global GST classification map was created, which is shown in Figure 1. The VIIRS GST data product may be downloaded from ftp://vct.geog.umd.edu/ST/.

3. Validation of the VIIRS global surface-type classification map

3.1. *Stratified random sampling and reference data*

Visual interpretation of high spatial resolution imagery was used to validate the VIIRS global classification product described above. Locations of the validation data set were selected through a stratified random sampling process. Stratified random sampling is a commonly used sampling method for validating global land cover products. For example, this technique has been used to validate the GLC2000 (Mayaux et al. 2006) and the

MODIS collection 5 land cover product (Friedl et al. 2010). Thorough studies have been conducted to evaluate this method (Olofsson et al. 2012; Stehman et al. 2012), and it has been proven to be effective. The stratified random sampling follows a probability sampling design that provides adequate sample size for rare land cover classes. In this study, IGBP classes were used as the strata in the stratification, and percentages of validation samples in different IGBP land cover classes, which were derived from Figure 1 of Olofsson et al. (2012), were used to allocate validation samples. In total, 5000 validation pixels were initially selected to represent the entire globe; 4958 points were taken into accuracy assessments and the rest were dropped due to uncertainties in interpretations. Sample sizes and distribution percentages are presented in Table 3.

Visual interpretation procedures were performed in an integrated validation tool, in which Google Map/Earth high spatial resolution images were retrieved as the primary reference data source. Other supplemental reference data, including archived Landsat images and other land cover products, such as MODIS collection 5 land cover and GLC2000 product, were also used. Class labels from other land cover products were checked to increase interpretation confidences in case qualities of reference images for interpretations were not high. To label a heterogeneous pixel, the corresponding ground area (1 km^2 for each pixel) in reference images was divided into 25 equal subareas (dynamically overlaid 5 × 5 grid) in the validation tool interface to help interpreters to determine the dominant land cover type on the ground, which was taken as the reference class label.

3.2. *Validation results*

Error matrices were used to assess the classification performance in this study, which was also used in the validation of the MODIS collection 5 land cover product. Other studies, such as Zhu et al. (2000), used map category marginal frequencies-based error matrix to evaluate classification accuracies (Card 1982), in which proportions of areas for each class in classification maps and statistical sampling designs were taken into probabilistic estimates. In this study, the error matrix of estimated proportions of area alongside estimated overall, user's and producer's accuracy and their corresponding standard errors are generated and presented in Table 4. The equations used here for the stratified random sampling design were introduced in Olofsson et al. (2014; eq. (4)-(7)) and Card (1982). The proportions of area per class, which are essential for the calculation, are listed in Table 3. The estimated overall accuracy calculated from the error matrix of estimated proportions of area is (78.64 ± 0.57)%.

3.3. *Analyses*

As shown in Table 4, high user's and producer's accuracy were achieved for the snow and ice, barren and evergreen broadleaf forests classes. Because the spectral characteristics of these classes are quite distinctive, it was not surprising that high classification accuracies were achieved. Above or close to 70% user's and producer's accuracies were obtained for both the evergreen needleleaf forests and the deciduous needleleaf forests classes; most misclassified pixels for these two classes belonged to mixed forests or woody savannahs. Mixed forests are very difficult to be accurately classified because the

Table 4. Error matrix of estimated area proportions (in percentage).

Classification	Reference 1	2	3	4	5	6	7	8	9	10	11	12	13	14	15	16	Total (%)	User's accuracy (%)	Producer's accuracy (%)
1	1.55	0	0.04	0.03	0.32	0	0.01	0.21	0.04	0.01	0.01	0.01	0	0	0	0	2.24	69.12 ± 3.24	79.32 ± 3.97
2	0	8.70	0	0.08	0.19	0	0	0.45	0.19	0	0	0.02	0	0.06	0	0	9.68	89.88 ± 1.33	95.06 ± 0.99
3	0.05	0	0.96	0	0.09	0.01	0	0.12	0.01	0	0	0	0	0	0	0	1.24	77.08 ± 4.31	65.02 ± 5.17
4	0	0	0.01	0.63	0.04	0	0	0.06	0.05	0.01	0	0	0	0.02	0	0	0.81	77.33 ± 3.43	27.86 ± 2.96
5	0.16	0.06	0.37	0.96	3.64	0	0	0.73	0.12	0.04	0	0.02	0.02	0.16	0	0	6.28	57.93 ± 2.81	73.63 ± 2.90
6	0	0	0	0	0	0.05	0.01	0	0	0	0	0	0	0	0	0	0.06	74.19 ± 4.56	4.43 ± 0.91
7	0.06	0	0	0.03	0.12	0.52	12.38	0.15	0.09	1.69	0.12	0.40	0.03	0.28	0	0.74	16.64	74.44 ± 1.88	89.29 ± 1.26
8	0.08	0.18	0.08	0.31	0.28	0.10	0.10	5.80	0.91	0.13	0.02	0.16	0.03	0.49	0	0	8.65	67.04 ± 2.04	63.16 ± 2.32
9	0	0.10	0	0.03	0.07	0.17	0.24	0.93	5.88	0.28	0	0.17	0.03	0.48	0	0	8.39	70.08 ± 2.94	70.38 ± 2.47
10	0.02	0	0	0.06	0.05	0.17	0.75	0.20	0.32	6.08	0	0.69	0.03	0.21	0	0.23	8.78	69.23 ± 1.91	66.36 ± 2.38
11	0.02	0	0	0.02	0.09	0	0.09	0.04	0.09	0.04	0.74	0.02	0	0	0	0	1.15	64.15 ± 6.65	81.34 ± 6.75
12	0.01	0	0.01	0.04	0.02	0.01	0.05	0.05	0.18	0.49	0.02	6.02	0.08	0.61	0	0	7.59	79.37 ± 1.44	75.78 ± 2.01
13	0	0	0	0	0	0	0	0.01	0	0	0	0.04	0.34	0.02	0	0	0.43	79.21 ± 4.06	57.26 ± 7.19
14	0	0.11	0.01	0.07	0.05	0.01	0.09	0.43	0.47	0.23	0	0.33	0.03	2.46	0	0.01	4.29	57.46 ± 2.34	51.46 ± 3.06
15	0	0	0	0	0	0	0	0	0	0	0	0	0	0	10.88	0	10.88	100 ± 0.00	100 ± 0.00
16	0	0	0	0	0	0	0.15	0	0	0.15	0	0.05	0	0	0	12.53	12.89	97.21 ± 1.04	92.76 ± 1.17
Total	1.95	9.15	1.47	2.25	4.94	1.04	13.87	9.18	8.35	9.16	0.91	7.95	0.59	4.79	10.88	13.50	100		

Note: Overall accuracy is (78.64 ± 0.57)%.

spectral and temporal feature of this type is relatively ambiguous. Therefore, confusion between mixed forests and other woody cover types, such as other forest classes and woody savannahs, was to be expected.

Closed shrublands and open shrublands presented similar user's accuracy, but many closed shrublands pixels were incorrectly classified, mainly as open shrublands. Some confusion regarding closed or open shrublands pixels with grasslands was also observed. Portions of savannah pixels in the validation were misclassified as woody savannahs and the cropland/natural vegetation mosaic classes. The confusion with woody savannahs is understandable because the thematic 'distance' between these two classes is close. The confusion with cropland/natural vegetation mosaic can be explained by these two classes sharing very heterogeneous spatial patterns.

The landscape of grasslands may vary significantly in different areas. Some sparse grasslands pixels in dry areas may be easily confused with open shrublands; other dense grasslands, which have similar spectral and temporal features, tend to be misclassified as croplands. The permanent wetland class is generally difficult to be accurately classified because shallow water mixed with vegetative cover tends to be confused with inland water and herbaceous vegetation. However, the validation result suggested that the classification of permanent wetland was better than expected.

Because a large number of croplands training samples have been carefully selected in various agricultural areas to help increase the representativeness of croplands characteristics, and further post-classification processes have been applied for the croplands class, satisfactory classification accuracy for this class has been achieved according to the validation. However, the user's and producer's accuracy for the cropland/natural vegetation mosaics were significantly lower than those from the croplands class, which might be explained by the highly heterogeneous nature of this mosaic class.

4. Conclusion

In this study, the processes of development and validation of the new VIIRS global GST classification map are introduced. The MODIS land cover heritage classification algorithm was adopted by the new product, but different annual metrics and processing steps were applied. Stratified random sampling was used to select validation points, and error matrices were used to evaluate the classification performance. The validation result suggested that (78.64 ± 0.57)% overall accuracy was obtained, which exceeded the 70% correct rate threshold in the JPSS Level 1 requirements document. Compared to accuracies of existing land cover products (67–68% for IGBP-DISCover and GLC2000 (Herold et al. 2008; Mayaux et al. 2006) and around 75% for MODIS collection 5 (Friedl et al. 2010)), the classification accuracy of the new VIIRS surface-type map is comparable to the accuracy of the MODIS land cover map and exceeds those from the IGBP-DISCover and GLC2000 products.

Acknowledgement

We thank the anonymous reviewers for the comments that helped improve the manuscript.

Disclosure statement

No potential conflict of interest was reported by the authors.

Funding

We would like to acknowledge all supports provided by the NOAA-NASA JPSS program office and the NOAA/NESDIS/STAR JPSS management team.

ORCID

Chengquan Huang http://orcid.org/0000-0003-0055-9798

References

Bartholomé, E., and A. S. Belward. 2005. "GLC2000: A New Approach to Global Land Cover Mapping from Earth Observation Data." *International Journal of Remote Sensing* 26 (9): 1959–1977. doi:10.1080/01431160412331291297.

Card, D. H. 1982. "Using Known Map Category Marginal Frequencies to Improve Estimates of Thematic Map Accuracy." *Photogrammetric Engineering and Remote Sensing* 48 (3): 431–439.

Carroll, M. L., J. R. Townshend, C. M. DiMiceli, P. Noojipady, and R. A. Sohlberg. 2009. "A New Global Raster Water Mask at 250 M Resolution." *International Journal of Digital Earth* 2 (4): 291–308. doi:10.1080/17538940902951401.

Cramer, W., D. W. Kicklighter, A. Bondeau, B. Moore Iii, G. Churkina, B. Nemry, A. Ruimy, A. L. Schloss, and The participants of the Potsdam NPP Model Intercomparison. 1999. "Comparing Global Models of Terrestrial Net Primary Productivity (NPP): Overview and Key Results." *Global Change Biology* 5 (S1): 1–15. doi:10.1046/j.1365-2486.1999.00009.x.

Feddema, J. J. 2005. "The Importance of Land-Cover Change in Simulating Future Climates." *Science* 310 (5754): 1674–1678. doi:10.1126/science.1118160.

Freund, Y., and R. E. Schapire. 1997. "A Decision-Theoretic Generalization of On-Line Learning and an Application to Boosting." *Journal of Computer and System Sciences* 55 (1): 119–139. doi:10.1006/jcss.1997.1504.

Friedl, M. A., D. Sulla-Menashe, B. Tan, A. Schneider, N. Ramankutty, A. Sibley, and X. Huang. 2010. "MODIS Collection 5 Global Land Cover: Algorithm Refinements and Characterization of New Datasets." *Remote Sensing of Environment* 114 (1): 168–182. doi:10.1016/j.rse.2009.08.016.

Friedlingstein, P., P. Cox, R. Betts, L. Bopp, W. Von Bloh, V. Brovkin, P. Cadule, et al. 2006. "Climate–Carbon Cycle Feedback Analysis: Results from the C ^{4} MIP Model Intercomparison." *Journal of Climate* 19 (14): 3337–3353. doi:10.1175/JCLI3800.1.

Hansen, M. C., R. S. Defries, J. R. G. Townshend, and R. Sohlberg. 2000. "Global Land Cover Classification at 1 Km Spatial Resolution Using a Classification Tree Approach." *International Journal of Remote Sensing* 21 (6–7): 1331–1364. doi:10.1080/014311600210209.

Herold, M., P. Mayaux, C. E. Woodcock, A. Baccini, and C. Schmullius. 2008. "Some Challenges in Global Land Cover Mapping: An Assessment of Agreement and Accuracy in Existing 1 Km Datasets." *Remote Sensing of Environment* 112 (5): 2538–2556. doi:10.1016/j.rse.2007.11.013.

Holben, B. N. 1986. "Characteristics of Maximum-Value Composite Images from Temporal AVHRR Data." *International Journal of Remote Sensing* 7 (11): 1417–1434. doi:10.1080/01431168608948945.

Lee, T. E., S. D. Miller, F. Joseph Turk, C. Schueler, R. Julian, S. Deyo, P. Dills, and S. Wang. 2006. "The NPOESS VIIRS Day/Night Visible Sensor." *Bulletin of the American Meteorological Society* 87 (2): 191–199. doi:10.1175/BAMS-87-2-191.

Loveland, T. R., Z. Zhu, D. O. Ohlen, J. F. Brown, B. C. Reed, and L. Yang. 1999. "An Analysis of the IGBP Global Land-Cover Characterization Process." *Photogrammetric Engineering and Remote Sensing* 65 (9): 1021–1032.

Mayaux, P., H. Eva, J. Gallego, A. H. Strahler, M. Herold, S. Agrawal, S. Naumov, et al. 2006. "Validation of the Global Land Cover 2000 Map." *IEEE Transactions on Geoscience and Remote Sensing* 44 (7): 1728–1739. doi:10.1109/TGRS.2006.864370.

NOAA. 2014a. *Joint Polar Satellite System (JPSS) VIIRS Surface Type Algorithm Theoretical Basis Document (ATBD)*. NOAA. http://www.star.nesdis.noaa.gov/jpss/documents/ATBD/D0001-S001-4006_ATBD_VIIRS-Surface-Type_A.pdf

NOAA. 2014b. *Joint Polar Satellite System (JPSS) Program Level 1 Requirements*. NOAA. http://www.jpss.noaa.gov/pdf/L1RDS_JPSS_REQ_1002_NJO_v2.10_100914_final-1.pdf

Olofsson, P., G. M. Foody, M. Herold, S. V. Stehman, C. E. Woodcock, and M. A. Wulder. 2014. "Good Practices for Estimating Area and Assessing Accuracy of Land Change." *Remote Sensing of Environment* 148 (May): 42–57. doi:10.1016/j.rse.2014.02.015.

Olofsson, P., S. V. Stehman, C. E. Woodcock, D. Sulla-Menashe, A. M. Sibley, J. D. Newell, M. A. Friedl, and M. Herold. 2012. "A Global Land-Cover Validation Data Set, Part I: Fundamental Design Principles." *International Journal of Remote Sensing* 33 (18): 5768–5788. doi:10.1080/01431161.2012.674230.

Pittman, K., M. C. Hansen, I. Becker-Reshef, P. V. Potapov, and C. O. Justice. 2010. "Estimating Global Cropland Extent with Multi-Year MODIS Data." *Remote Sensing* 2 (7): 1844–1863. doi:10.3390/rs2071844.

Quinlan, J. R. 1993. *C4.5: Programs for Machine Learning*. The Morgan Kaufmann Series in Machine Learning. San Mateo, Calif: Morgan Kaufmann Publishers.

Quinlan, J. R. 2004. "Data Mining Tools see5 and C5.0 (version 2.10)." Windows, Linux. Rulequest Research. http://rulequest.com/see5-info.html

Schneider, A., M. A. Friedl, and D. Potere. 2009. "A New Map of Global Urban Extent from MODIS Satellite Data." *Environmental Research Letters* 4 (4): 044003. doi:10.1088/1748-9326/4/4/044003.

Stehman, S. V., C. E. Pontus Olofsson, M. H. Woodcock, and M. A. Friedl. 2012. "A Global Land-Cover Validation Data Set, II: Augmenting a Stratified Sampling Design to Estimate Accuracy by Region and Land-Cover Class." *International Journal of Remote Sensing* 33 (22): 6975–6993. doi:10.1080/01431161.2012.695092.

Zhu, Z., L. Yang, S. V. Stehman, and R. L. Czaplewski. 2000. "Accuracy Assessment for the U.S. Geological Survey Regional Land-Cover Mapping Program: New York and New Jersey Region." *Photogrammetric Engineering and Remote Sensing* 66 (12): 1425–1438.